JGR Space Physics

RESEARCH ARTICLE
10.1029/2019JA026780

On the Sources of the Ionospheric Variability in the South American Magnetic Anomaly During Solar Minimum

J. Moro[1,2], J. Xu[1], C. M. Denardini[3], L. C. A. Resende[3], R. P. Silva[3], Z. Liu[1], H. Li[1], C. Yan[1], C. Wang[1], and N. J. Schuch[2]

[1]State Key Laboratory of Space Weather, Beijing, China, [2]Southern Regional Space Research Center—CRCRS/COCRE/INPE-MCTIC, Santa Maria, Brazil, [3]National Institute for Space Research—INPE/MCTIC, São José dos Campos, Brazil

Key Points:
- Recent Digisonde observations at Santa Maria has enabled this first study of ionospheric variability in the central region of the SAMA
- The relative standard deviation is used as a quantitative measurement of the f_oE, f_oF_2, h_mF_2, and $B0$ variability
- $B0$ is the most variable parameter, while f_oE is the least variable; f_oF_2 is much more variable than h_mF_2

Correspondence to:
J. Moro,
juliano.moro@inpe.br

Citation:
Moro, J., Xu, J., Denardini, C. M., Resende, L. C. A., Silva, R. P., Liu, Z., et al. (2019). On the sources of the ionospheric variability in the South American Magnetic Anomaly during solar minimum. *Journal of Geophysical Research: Space Physics*, *124*, 7638–7653. https://doi.org/10.1029/2019JA026780

Received 29 MAR 2019
Accepted 14 AUG 2019
Accepted article online 28 AUG 2019
Published online 5 SEP 2019

Abstract We investigate for the first time the variability of the F_2 layer critical frequency (f_oF_2), its peak height (h_mF_2), the thickness parameter $B0$, and the E region critical frequency (f_oE) over Santa Maria (29.7° S, 53.7° W, dip angle = −37°), a station located in the central region of the South American Magnetic Anomaly. The selected ionospheric parameters were obtained from ionograms recorded by a recent Digisonde Portable Sounder 4-D. The time period covers 309 days from 1 September 2017 to 30 August 2018. The diurnal analyses revealed a large day-to-day ionospheric variability, with some peculiarities as a strong semiannual pattern superimposed to expected ionospheric behavior. Furthermore, the results show significant differences between the averaged f_oF_2 in December and June solstices, revealing a possible presence of the annual asymmetry. The coefficient of variation (CV) is used as a quantitative description of the variability of each parameter versus time and season. Considering low solar flux and geomagnetically quiet days only, we note that CV is smaller during the daytime and larger during nighttime for all parameters. The least variable ionospheric parameter in our study is f_oE, while the most variable one is $B0$. Regarding the F_2 layer parameters, we observe that f_oF_2 is much more variable than h_mF_2. We attribute the observed CV to the neutral atmosphere source over Santa Maria. The ionospheric variability is in general enhanced during geomagnetically disturbed periods. The estimated CV is higher over Santa Maria than Wuhan, China (30.5° N, 114.4° E, dip angle = 46°), a station with no influence of the South American Magnetic Anomaly.

1. Introduction

It is well established that production, loss, and transport processes that occur in the ionosphere is subject to many influences from the Sun, magnetosphere, and lower and middle atmosphere, which deviate it from the climatological mean. This deviation is broadly known as ionospheric variability and can occur on hourly, daily, seasonally, and solar cycle time scales (Araujo-Pradere et al., 2005; Forbes et al., 2000; Rishbeth & Mendillo, 2001; Zhang & Holt, 2008). Rishbeth and Mendillo (2001) describe the possible causes of ionospheric variability into four categories: (i) solar ionizing radiation (solar flares, 27-day solar rotation, formation and decay of active regions, 11-year solar cycle, and solar zenith angle dependence), (ii) solar wind-geomagnetic activity (substorms, geomagnetic storms, energetic particle precipitation, and Joule heating), (iii) neutral atmosphere-meteorological (through the upward propagating waves like planetary, tidal, gravity, and infrasonic waves and their modulations), and (iv) electrodynamics (prompt penetration electric field, plasma convection at high latitude, and electric fields from lightning sprites). All these sources of ionospheric variabilities impose certain challenges for studying and/or modeling the ionosphere that may improve existing models. Once ionospheric measurements are usually limited in space and time, any quantitative measurements of the ionospheric variability using some of the most important parameters of the E and F regions have been an important part of space weather research and modeling. Such measurements are especially important when the region under study encompasses certain regional peculiarities like the South American Magnetic Anomaly (SAMA; Abdu et al., 2005).

Several authors have studied the ionospheric deviation using different methods and parameters for determining the variability. Forbes et al. (2000) obtained some estimates of how ionospheric variability is divided between solar ionizing flux, solar wind conditions, and neutral atmosphere influences. The authors found that the daily fluctuations in the peak electron density of the F_2 layer (N_mF_2) under quiet geomagnetic conditions range from 25% to 35% at periods from few hours to 1–2 days and vary between 15% and 20% at periods from 2 to 30 days. They assumed that these fluctuations are due the neutral atmosphere sources since the

deviation of solar flux variation is small within these time scales. The authors analyzed separated zones of latitude without considering fluctuations by daytime/nighttime periods or by seasons. Such diurnal/nocturnal period and seasonal ionospheric variability study was made by Rishbeth and Mendillo (2001). They found that the N_mF_2 variability is greater by night than at day and greater at equinox than at solstice months. It is also higher at subauroral and equatorial latitudes than at midlatitudes.

Some other major efforts to study the *E* and *F* regions variabilities were conducted over several regions, most of them in the Northern Hemisphere (Abe et al., 2013; Akala et al., 2010; Bilitza et al., 2004; Medvedeva & Ratovsky, 2015; Somoye & Akala, 2011; Tsagouri et al., 2018; Zhang et al., 2004; Zhang & Holt, 2008). In the South American sector, the short-term variabilities (few days in 2002) of the F_2 peak parameters were discussed based on data collected in three Conjugate Point Equatorial Experiment (COPEX) station, Boa Vista (2.8° N, 60.7° W, dip angle = 22°), Cachimbo (9.5° S, 54.8° W, dip angle = −4°), and Campo Grande (20.5° S, 55° W, dip angle = −22°), by Abdu et al. (2009) and McNamara et al. (2008). Moreover, Batista and Abdu (2004) analyzed the parameters f_oF_2, h_mF_2, and $B0$ obtained by digital ionosondes over two stations in Brazil, São Luís (2.6° S, 44.2° W, dip angle = −0.5°) at the magnetic equator and Cachoeira Paulista (22.7° S, 45° W, dip angle = −28°), close to the southern crest of the Equatorial Ionization Anomaly (EIA). The authors compared their observational data with the modeled results by International Reference Ionosphere, in which it showed some discrepancies in specific hours. Recently, Romero-Hernandez et al. (2018) studied the day-to-day variation of the ionosphere in the Northern and Southern Hemispheres over the Latin American sector but using daytime total electron content variation. However, the previous mentioned works in the South America sector did not explore or discussed the dispersion of ionospheric data from their mean values qualitatively.

To the best of author's knowledge, it seems that the prior studies about ionospheric variabilities using ionosonde data have focused in *F* region parameters collected in the Northern Hemisphere, equatorial region in Africa, or fall within borders to one of the crests of the EIA. Moreover, no previous work appears to have examined simultaneously the variabilities in the *E* and *F* region parameters. It is noted that the ionospheric variability would be understood more when the *E* region is studied simultaneously with the *F* region parameters. Therefore, there exists a gap in proper understanding the ionospheric variability in South America, especially in the Brazilian sector where there are some unique geophysical characteristics. One of them is the high magnetic declination angle that reaches approximately −20° in the equatorial region due to the dip equator secular displacement effect causing considerable changes in the Equatorial Electrojet and consequently in sporadic E (Es) layers (Denardini et al., 2018; Moro et al., 2016a, 2016b; Moro et al., 2017; Resende et al., 2016). There is also a more pronounced energetic particle precipitation in the SAMA region (Moro et al., 2013, 2012) when compared with other regions having the same latitudinal range, due to the global minimum in the intensity of the geomagnetic field.

Thus, this paper uses, for the first time, data acquired by a Digisonde Portable Sounder 4-D (DPS-4D) recently installed at Santa Maria (29.7° S, 53.7° W, dip angle = −37°), a low latitude station located close to the center of the SAMA. The period of study covers 309 days from 1 September 2017 to 30 August 2018, which is characterized by low solar activity with few geomagnetically disturbed days. We use the coefficient of variation (CV) as an index of variability of f_oF_2, f_oE, h_mF_2, and $B0$, which will be defined in next section, to study their detailed behaviors in the SAMA region. The results obtained over Santa Maria is compared with the ionospheric data acquired by a DPS-4D installed at the Wuhan Ionospheric Observatory, China (30.5° N, 114.4° E, dip angle = 46°), a station with no influence of the SAMA. The positions of Santa Maria and Wuhan are marked by the black stars in the map of Figure 1. The solid black line across the continents is the geomagnetic equator. In addition, we included the locations of several other stations that will be mentioned in the discussions. Therefore, the main objectives of this work are (1) to discuss the characteristics of the data and the system recently installed in Santa Maria, (2) to analyze the diurnal and seasonal patterns of the ionospheric variability through the selected parameters for the whole year of data, (3) to analyze the sources of ionospheric variability over Santa Maria, (4) to compare the results over Santa Maria with Wuhan during two geomagnetic storms, and (5) to discuss the physical reasons of the obtained results.

2. Data and Method of Analysis

A new DPS-4D or Digisonde (Reinisch et al., 2009) is operating at the campus of the Federal University of Santa Maria (UFSM), Santa Maria, Brazil, since April 2017, under the support of the Space Weather

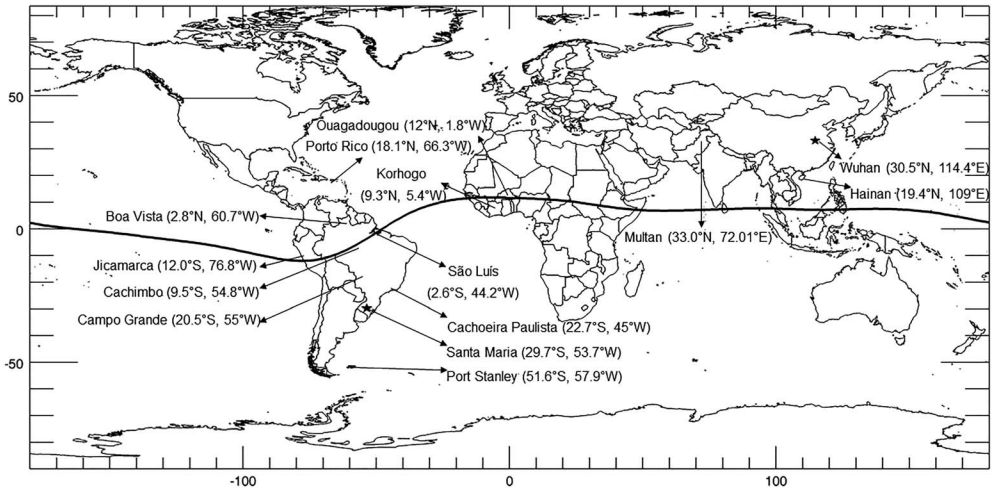

Figure 1. The black stars mark the positions of the Santa Maria and Wuhan stations. The locations of several other stations used in the discussions are also included. The solid black line represents the geomagnetic equator.

Monitoring Meridian Project of China (Wang, 2010), the Brazilian Study and Monitoring of Space Weather (Embrace) Program from the Brazilian National Institute for Space Research (INPE/MCTIC), and Federal University of Santa Maria. The system fills a gap of ionospheric sounders operating in real time between the Cachoeira Paulista station and the Port Stanley station (51.6° S, 57.9° W, dip angle = −49.8º), located in Argentina, as can be seen in Figure 1. The Digisonde in Santa Maria is set to transmit radio waves continuously into ionosphere from 1 MHz and increases the frequency up to 20 MHz with the sweep rate of 25 kHz for each round. The train of echoes to form an ionogram is transmitted/received with a 5-min time resolution.

An example of the daytime ionogram collected at Santa Maria station at 18:00 universal time (UT) on 12 July 2017 is shown in Figure 2. The local time (LT) is LT = UT − 3 hr. The modern ionosondes like the DPS-4D measure the polarization of the received signals identifying the O and X echoes by the red and green pixels as labeled in the figure. The critical frequencies obtained from ionograms provide direct measurements of electron density at the layer peak. In the example ionogram, the lower penetration frequency for the F_2 region, f_oF_2 is 6.10 MHz. Thus, the electron density at the F_2 layer peak can directly be obtained by $N_mF_2\ (el\ \ m^3) = 1.24 \times 10^{10}\ (f_oF_2/\mathrm{MHz})^2$. On the other hand, the altitude of the density peak of F_2 layer, h_mF_2, is not measured directly (Huang & Reinisch, 2001), but it can be obtained after processing analysis. In the example ionogram, its value is 222.8 km.

The lower penetration frequency for the E region, f_oE, is 2.9 MHz for the case shown in Figure 2. The physics involved in this region is simpler than for the F region, and its main features are well described by the Chapman theory (Hargreaves, 1995). The f_oE presents a well-known variation with the solar zenith angle and satisfies $f_oE = A\ (cos\chi)^{0.25}$, where A is determined by electron production and loss rate (Titheridge, 2000).

In addition to the E and F layers, Figure 2 also shows the calculated vertical electron density profile. The α-Chapman estimate of the F_2 layer topside is shown as the dashed black line. We also choose to analyze the parameter $B0$ since it provides a measure of the thickness of the bottomside profile and it is used in the empirical models like the International Reference Ionosphere. $B0$ is calculated as the height difference between h_mF_2 and the height where the electron density has dropped to $0.24 \times N_mF_2$ (Bilitza et al., 2000).

Other features usually observed in the ionograms collected in Santa Maria are the skywave signals sent by the Digisonde installed at Campo Grande station. The traces between 10 and 13.5 MHz are the oblique incidences from Es, F_1, and F_2 layers, identified as 1-hop E Es, 1-hop F1, and 1-hop F2, respectively. Our ionograms can therefore simultaneously register the vertical incidence and oblique incidence traces. However, the system is limited to automatically identify signals arriving within zenith angles of less than 15° as vertical incidence and those with zenith angles larger than 15° as oblique incidence. The automatic program simply disregards any signal flagged as oblique incidence.

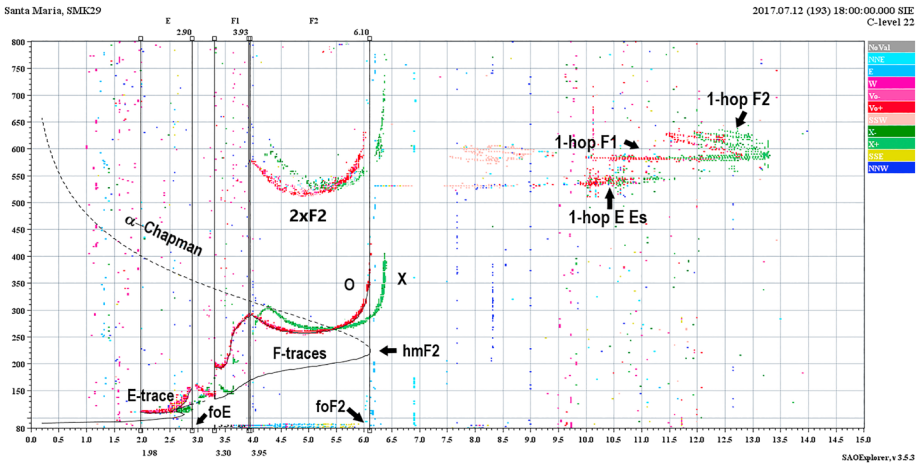

Figure 2. Daytime ionogram at Santa Maria collected at 18:00 universal time (15:00 local time) on 12 July 2017.

All recorded ionograms used in this work are initially auto-scaled by the Automatic Real Time Ionogram Scaler with True Height integrated into the Digisonde Ionogram Data Visualization/Editing Tool (SAO Explorer) developed by the Center for Atmospheric Research, University of Lowell Massachusetts. Nevertheless, in order to obtain reliable f_oF_2, f_oE, h_mF_2, and $B0$ parameters, each ionogram was checked and manually edited. The reason is that the high magnetic declination angle, which is a peculiarity in the Brazilian sector, affects the physics of the E and F layers development (Moro et al., 2017), controlling the F layer dynamo development in evening hours (Abdu et al., 2005). Therefore, manual scaling is a wide technique used in ionograms collected in Brazil to achieve a good quality of ionospheric parameters.

In order to quantify the ionospheric variability over Santa Maria, which is the focus of this paper, we use two methods for analyzing the data: (1) using the mean values approach and (2) using the CV, also known as relative standard deviation, as an index of variability. The CV has been used for several authors to express the variability in the ionospheric parameters (Akala et al., 2010; Forbes et al., 2000; Rishbeth & Mendillo, 2001; Somoye & Akala, 2011; Tsagouri et al., 2018; Zhang & Holt, 2008, among others). The CV is statistically defined in Equation (1) as

$$CV\ (\%) = \left(\frac{\sigma}{\mu}\right)\times 100 \tag{1}$$

In this equation, the standard deviations (σ) and the mean (μ) values of the parameters f_oF_2, f_oE, h_mF_2, and $B0$ calculated for certain time intervals are used to obtain the respective percentage relative standard deviation: f_oF_2 CV (%), f_oE CV (%), h_mF_2 CV (%), and $B0$ CV (%).

The seasonal effects are studied in this work by using the mean and standard deviation data from 3 months that make up each season as follow: December solstice (73 days of November, December, and January), March equinox (65 days of February, March, and April), June solstice (80 days of May, June, and July), and September equinox (91 days of August, September, and October). The solar emission at the wavelength of 10.7 cm ($F_{10.7}$, measured in 10^{-22} Wm^{-2} Hz^{-1}) and geomagnetic activity index Kp, for looking at their influence in the ionospheric variability, if any, are provided online (https://omniweb.gsfc.nasa.gov/form/dx1.html).

In the next section, we discuss the diurnal and seasonal patterns of f_oF_2, f_oE, h_mF_2, and $B0$ observed in the central region of the SAMA during the last solar minimum (2017–2018). In the following, we quantify the ionospheric variability through the CV during geomagnetically quiet days. At last, we show two case studies considering the CV calculated for geomagnetically disturbed days. The results obtained for Santa Maria are compared with the CV estimated from ionospheric data acquired in Wuhan, a station with no influence of the both SAMA and EIA.

3. Results and Discussion

3.1. Diurnal and Seasonal Variations of the Ionospheric Parameters Over Santa Maria

An overview of the f_oF_2, f_oE, h_mF_2, and $B0$ observed over Santa Maria is depicted in Figure 3. The mass plots in the left panels display 309 single days variations from 1 September 2017 to 30 August 2018 of the f_oF_2 and f_oE parameters in megahertz and h_mF_2 and $B0$ parameters in kilometer from top to bottom. The diurnal variation of these parameters in the seasonal scales are presented in the right panels of Figure 3. The UT runs along the horizontal axes, and the LT scale is at the top of the Figures 3a and 3e.

The sunrise varied from 9:15 UT to 10:30 UT from 1 September 2017 to 30 August 2018 over Santa Maria, while the sunset took place between 20:43 UT and 23:39 UT. Therefore, we consider daytime hours from 9:00 UT (06:00 LT) to 21:00 UT (18:00 LT). The number of data available during nighttime hours is small as compared to the daytime hours. This is due to the occurrence of spread F at night, which manifest as diffused echoes on the ionograms after sunset. The spread F may be associated to the plasma bubble occurrences, regions in the ionospheric plasma where the electron density is reduced due to the Rayleigh-Taylor instability process (Abdu, 2001).

It can be seen from Figure 3 that all parameters show diurnal and a large day-to-day variability during all seasons. We observe some peculiarities in the ionospheric parameters superimposed to expected ionospheric behavior already described in preview works. One of the peculiarities seen in the diurnal variations of f_oF_2 is the strong semiannual pattern, which is the larger f_oF_2 values for equinoxes than for solstices. From the left panels, we observe an exceptionally high afternoon variation with few observations from 6 to 9 MHz between 14:00 UT and 22:00 UT. The high afternoon variability between 250 and 300 km in h_mF_2 is slightly seems in a shorter period, from 14:00 UT to 19:00 UT. The diurnal variation patterns show that f_oF_2, f_oE, and $B0$ are higher during daytime hours, while the opposite holds for nighttime hours. Regarding the h_mF_2 values, it presents, in general, opposite behavior. The nighttime values are higher than those of the daytime values except for periods around 9:00 UT in June solstice and around 14:30 UT in December solstice. It is also remarkable the mean differences between December (red dots) and June (black dots) solstices, which are presented in all parameters in the right panels, reveal a possible presence of the annual asymmetry (sometimes called by annual or nonseasonal anomaly). The annual asymmetry, in the world as a whole, is an annual variation of the maximum electron density approximately 20% greater in December than in June (Rishbeth & Müller-Wodarg, 2006; Zou et al., 2000). A subtle difference between March (green dots) and September (blue dots) equinoxes during the afternoon has also been detected.

The general behavior of f_oF_2 presented in Figures 3a and 3e shows clearly that the diurnal trend depends upon the rotation of the Earth through the photoionization process of the neutral atmosphere by solar radiation. The plasma production is small at night if there is no energetic particle precipitation in the SAMA region (Moro et al., 2013). The lowest predawn values of f_oF_2 occur between 8:00 UT and 9:00 UT, while its daytime local maxima are observed in the afternoon with time depending the season. The post-sunrise increase is observed in all the seasons until pronounced peaks of 10.2 ± 1.0 MHz at 19:00 UT in December solstice, 9.3 ± 1.3 MHz at 18:15 UT in March equinox, and 8.8 ± 2.3 MHz at 17:25 UT in September equinox. The f_oF_2 peak is not clearly identified in June solstice because the afternoon pattern is almost flat from 14:00 UT to 20:00 UT, but it occurs at 18:15 UT with a magnitude of 5.7 ± 1.0 MHz. After the peaks, the f_oF_2 values decrease until sunset time and keep decreasing onward, which is an effect of the absence of solar radiation that leads to an increase of the neutral density and chemical losses. This also explains the $B0$ behavior at night, as will be explained ahead. Quantitatively, f_oF_2 always stands below 14 MHz from 1 September 2017 to 30 August 2018. In fact, only in a few days, it exceeds 12 MHz, which are due to geomagnetically disturbed days. The highest value of 14 MHz corresponding to an electron density of 2.4×10^{12} electrons per m^3 is observed at 19:40 UT on 8 January 2018. The lowest value of f_oF_2 equal to 1.7 MHz, which corresponds to an electron density of 3.6×10^{10} electrons per m^3, is observed at 8:15 UT on 19 April 2018.

Since Santa Maria (−37° dip angle) lies outside of the expected position of the EIA peaks (between 15° and 20° from the equator), we observed lower f_oF_2 values compared to observations near the EIA crests. McNamara et al. (2008) determined the diurnal variations of the F_2 peak parameters for three Brazilians stations (see Figure 1) during the COPEX campaign of the Year 2002: Boa Vista (22° dip angle), Campo Grande

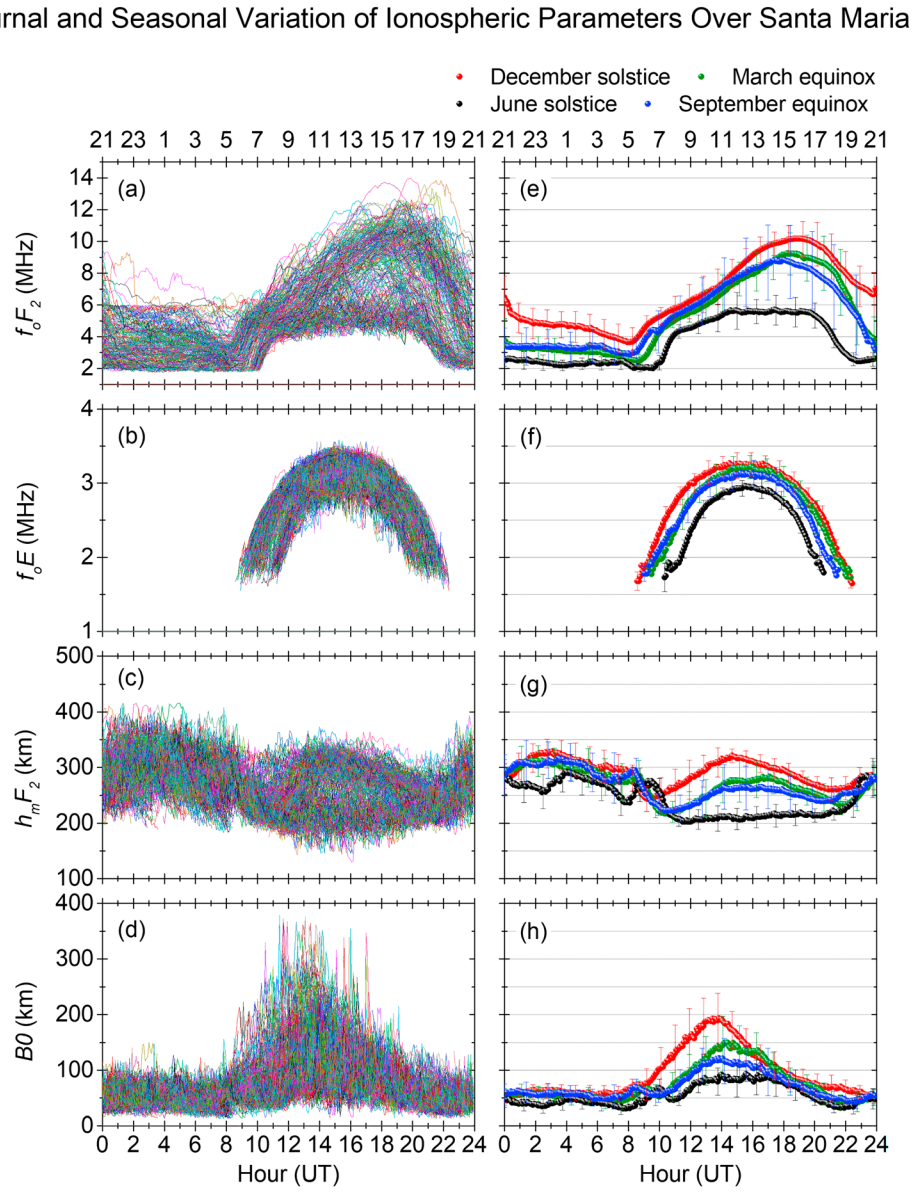

Figure 3. (a–d) Superposed single day plots of f_oF_2, f_oE, h_mF_2, and $B0$ from 1 September 2017 to 30 August 2018 sampled by the Santa Maria Digisonde Portable Sounder 4-D, as a function of universal time. (e–h) Monthly average of f_oF_2, f_oE, h_mF_2, and $B0$ parameters for December solstice (red dots), March equinox (green dots), June solstice (black dots), and September equinox (blue dots). The local time scale is at the top of the graphics in the first row.

(−22° dip angle), and Cachimbo (−4° dip angle). McNamara et al. (2008) observed a large amount of diurnal and day-to-day variability of f_oF_2. The Stations Boa Vista (outside of SAMA) and Campo Grande (SAMA boundary) located near the EIA crests presented the highest recorded values of f_oF_2 of around 21 MHz. On the other hand, the Cachimbo (SAMA boundary) station located close to the magnetic equator presented f_oF_2 values less than 16 MHz during the campaign. Recently, Bello et al. (2019) presented the response of the N_mF_2, h_mF_2, and $B0$ ionospheric to the Equatorial Electrojet at Jicamarca, Peru (12.0° S, 76.8° W, dip angle = −0.05°), away from the SAMA. Considering the results representing solar minimum, the authors reported that N_mF_2 reach peaks of 8.8×10^{11} electrons per m^3 (~8.5 MHz) during equinoxes, 9.5×10^{11} electrons per m^3 (~8.8 MHz) in summer, and 5.7×10^{11} electrons per m^3 (~6.8 MHz) in winter between 15:00 UT and 17:00 UT. Comparing the findings from other stations located in the boundary or outside the SAMA's control with our results, we found that a large amount of diurnal

and day-to-day variability in f_oF_2 is caused basically by the EIA influence and not by the presence of the SAMA. In other words, the effects of the EIA in the ionospheric parameters are more intense than the ones caused by the SAMA.

As can be noted from Figures 3b and 3f, the f_oE parameter presents a regular and smooth diurnal variation, increasing almost linear from sunrise to the peak in the afternoon and falling until sunset. In the nighttime hours, the detection of the E region is difficult under the condition of low electron density, and the Digisonde is not able to detect this layer. During geomagnetically disturbed days, which is not the case presented in Figure 3, it is possible to detect the E layer due to the presence of the SAMA. The diurnal variation of f_oE responds positively to the intensity of the Sun, which is a well-known characteristic of the E layer (Abe et al., 2013; Ouattara et al., 2009). The f_oE parameter also presents higher values during December solstice (3.3 ± 0.2 MHz at 14:30 UT), followed by March equinox (3.2 ± 0.2 MHz at 15:55 UT), September equinox (3.1 ± 0.2 MHz at 15:15 UT), and lower values on June solstice (2.9 ± 0.1 MHz at 15:30 UT). The highest value of 3.6 MHz is observed at 15:15 UT on 27 October 2017, and the minimum value of 1.5 MHz is detected at 8:55 UT on 16 January 2018.

Concerning the h_mF_2 presented in Figures 3c and 3g, we note a diurnal variation with higher values during nighttime hours and lower values during daytime hours. The increase of h_mF_2 values at nighttime hours is usually explained by the absence of plasma production and the relatively slow chemical recombination above ~200 km, similar behavior that appears over the Arecibo Observatory (18.1° N, 66.3° W, dip angle = 30°) as discussed by Gong et al. (2012). In addition to these factors, the nighttime increase in h_mF_2 values may be also explained by the action of equatorward meridional winds over Santa Maria, which pushes the electron density up along the magnetic field lines. Unfortunately, our study has been limited by uncertainties in the knowledge of the neutral wind in the subtropical region of Santa Maria. On the other hand, Kalita et al. (2015) studied the characteristics of the F_2 layer parameters over Dibrugarh (27.5° N, 95° E, dip angle = 43°), a midlatitude station in India. The authors pointed out that winds could be a dominant factor in the h_mF_2 behavior over Dibrugarh because the winds produce the maximum effects in height at this magnetic dip angle. As Santa Maria is located at a magnetic dip angle of −37°, there is a high probability that the effects of winds in the ionospheric F_2 height be a dominant mechanism for h_mF_2 behavior observed in our results. After midnight, the h_mF_2 values fall to lower altitudes where the neutral density and the chemical loss are greater and f_oF_2 and $B0$ also decreases. A precipitous decrease between 8:00 UT and 9:00 UT (when the solar zenith angle is greater) is observed in h_mF_2, except in June solstice because it occurs 1 hr earlier. The behavior of rapid ascent/descent may be explained by the increase of electron concentration near F_2 peak by solar radiation. Thus, the height of the F_2 layer shifts downward, showing a dip in the h_mF_2 due to the fast plasma production. This is also observed at Jicamarca by Lee and Reinisch (2012). We also observe a small increase in h_mF_2 soon after sunrise hours until noon especially in December solstice and equinoxes, while this increase is not evident in June solstice. The peaks may be explained in terms of the increase in the temperature due to daylight that increases the concentration of atomic oxygen, as explained by Ameen et al. (2018) from Digisonde data acquired at Multan (30.2° N, 71.5° S, dip angle = 47.4°). After the sunset period, when the rate of ion formation decreases, the height of F_2 layer increases toward midnight as described before, corresponding a decrease in f_oF_2 (or N_mF_2) as noted in Figures 3a and 3e. Regarding the maximum and minimum h_mF_2 values, we observe the highest value of 416 km at 01:20 UT on 14 October 2017, while the lowest value equal to 130 km is observed at 16:05 UT on 30 June 2018. Seasonally, the highest mean value of h_mF_2 in December solstice is 328.5 ± 24.6 km at 03:05 UT, in March equinox is 312.5 ± 27.3 km at 2:25 UT, in June solstice is 292.3 ± 28.6 km at 4:00 UT, and in September equinox is 316.9 ± 36.2 km at 3:30 UT.

From the diurnal variations of $B0$ presented in Figures 3d and 3h, we see that its values increase gradually from sunrise onward until a peak found to occur around local noon in equinoxes and less evident in June solstice. The peak happens earlier in December solstice. Thereafter, the mean values of $B0$ show a gradual fall. The minimum values appear in May and July around sunrise hours, months which h_mF_2 show the rapid ascent/descent. The maximum value of 378 km occurs at 11:25 UT on 23 December 2017. With a few exceptions, all the individual $B0$ values are below 100 km from 00:00 UT to 8:00 UT and above 300 km from 10:00 UT to 17:00 UT. The highest mean values of $B0$ in each season are 193.6 ± 50.3 km at 13:50 UT in December solstice, 149.5 ± 50.2 km at 14:20 UT in March equinox, 93.3 ± 43.8 km at 15:35 UT in June solstice, and 121.3 ± 42.8 km at 13:50 UT in September equinox.

Since N_mF_2 is proportional to $(f_oF_2)^2$, we note in Figure 3e a big difference in the F_2 layer ionization between December solstice months (November, December, and January) and June solstice months (May, June, and July). The difference between the mean f_oF_2 values in these months may be the annual asymmetry, but it can only be separated from the seasonal anomaly by combining data from opposite seasons in the two hemispheres, which it is not the focus of this work. Regarding the annual asymmetry that might be the case we are observing here, it is characterized by greater average N_mF_2 in December than June, both by day and by night (Zou et al., 2000). Rishbeth and Müller-Wodarg (2006) explained that a possible cause is the December/July variation of 3.5% in Sun-Earth distance and consequent 7% variation in the flux of ionizing radiation, associated with the asymmetries of the geomagnetic field and winds. We remind the reader that Santa Maria is located near the central region of the SAMA, that is, a region with big asymmetries in the geomagnetic field as compared with the Northern Hemisphere. In addition, Santa Maria is in the boundary of low and middle latitudes, and then the thermospheric meridional neutral wind affects the ionosphere in this latitude thought transport processes of the electric charges controlling the h_mF_2 (Balan et al., 1997; Liu et al., 2009). An upward (downward) plasma movement along the magnetic field lines is caused by an equatorward (poleward) wind (Batista et al., 1997; Romero-Hernandez et al., 2018; Shim et al., 2010). Therefore, changes in h_mF_2 will produce variations in N_mF_2 (due to changes in f_oF_2) as observed in our results from December solstice to June solstice in Figure 3e. We also note an equinoctial asymmetry after ~18:00 UT, with the ionization in March equinox being stronger than that in September equinox. Overall, we note from Figure 3 that the day-to-day variability is a permanent feature of the ionospheric E and F regions over Santa Maria.

3.2. Ionospheric Variabilities During Geomagnetically Quiet Days

In our attempt to study quantitatively the ionospheric variabilities and its main causes over Santa Maria, we may reduce the four possible sources described before to three broad categories: fluctuations of the solar ionizing radiation, geomagnetic activity, and by an internal process in the neutral atmosphere. Therefore, we discuss the relative contribution of these sources by using rough arguments based on observed solar emission and geomagnetic index data.

Regarding the first possible source of ionospheric variability, that is, the solar ionization radiation, we have an important advantage. The 1-year data used are characterized by a very low level of solar and magnetic activity. The average of the $F_{10.7}$ index from 1 September 2017 to 30 August 2018 is only $71.6 \pm 3.5 \times 10^{-22}$ Wm^{-2} Hz^{-1}. With the 27-day averaged values of $F_{10.7}$ (sunspot number) in the range 67.6–80.1 (1–18) in the period, the ionospheric data used in this work represent low solar activity. The variabilities that may be caused by variations in the $F_{10.7}$ are largely excluded in this work.

In order to exclude the geomagnetic activity impacts on the ionospheric variabilities and to estimate the variabilities due to the neutral atmosphere source, we evaluated the CV using equation (1) considering data acquired during geomagnetically quiet days ($Kp \leq 3$) only. The CV is calculated on an hourly basis, and the results are presented in Figure 4. The f_oF_2 CV, f_oE CV, h_mF_2 CV, and $B0$ CV on a seasonal scale presented from top to bottom should be mainly due to the meteorological sources. The diurnal variations of CV are not straightforward due to specific characteristics in each parameter, time, and season. In order to summarize its general characteristics, we present in Table 1 the minimum, maximum, average (μ), and corresponding standard deviations (σ) of f_oF_2 CV, f_oE CV, h_mF_2 CV, and $B0$ CV for each season.

The diurnal variations of f_oF_2 CV values presented in Figure 4a show that CV is over 10% in the predawn hours, decreases down during daytime hours, and then begins to increase in the equinox months toward the dusk. In December and June solstices, the f_oF_2 CV remains below 20% during nighttime hours. The minimum f_oF_2 CV is $5.6 \pm 2.26\%$ observed at 9:00 UT in June solstice, as shown in Table 1. In order to determine if the value $5.6 \pm 2.26\%$ is statistically significant different from the other minimum f_oF_2 CV values ($7.0 \pm 0.24\%$, $9.4 \pm 0.95\%$, and $19.6 \pm 0.65\%$), we performed the Kruskal-Wallis (Kruskal & Wallis, 1952) test. The results show that at the 0.05 level, the minimum f_oF_2 CV values are statistically different among them. The Kruskal-Wallis test was also performed in the maximum f_oF_2 CV values in Table 1 and showed that the distributions $23.0 \pm 1.28\%$, $38.5 \pm 1.36\%$, $19.0 \pm 1.21\%$, and $49.4 \pm 1.90\%$ are also statistically significantly different among them. Therefore, we can state that the f_oF_2 CV ranges from $5.6 \pm 2.26\%$ in June solstice to $49.4 \pm 1.90\%$ at 22:00 UT in September equinox, which is by far the most variable season with an average of $31.3 \pm 6.8\%$. June solstice presents the least f_oF_2 CV average equal to $13.4 \pm 2.8\%$. We also performed the

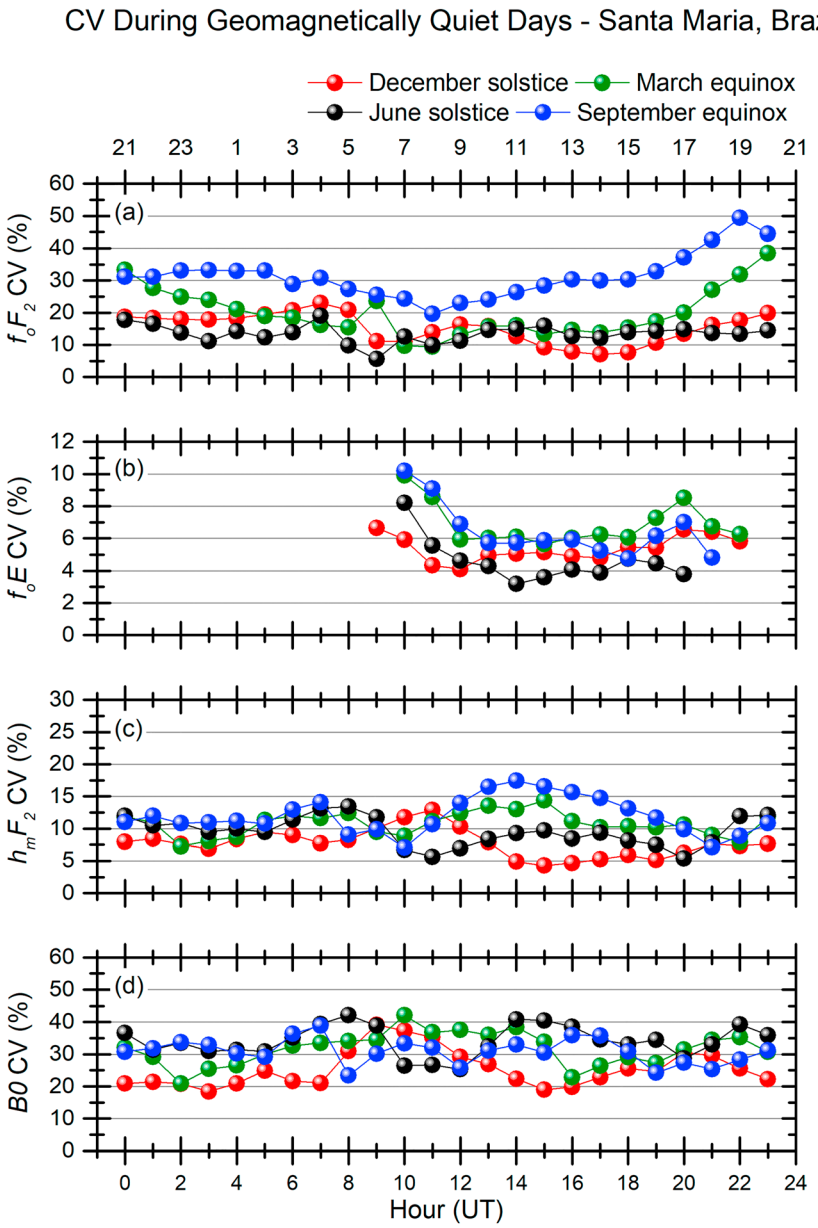

Figure 4. Coefficient of variability (CV) evaluated for the (a) f_oF_2, (b) f_oE, (c) h_mF_2, and (d) $B0$ parameters in December solstice (red dots), March equinox (green dots), June solstice (black dots), and September equinox (blue dots) as a function of universal time. The local time scale is at the top.

Kruskal-Wallis test considering the seasonal values for the remaining parameters in Table 1. We found that the maximum $B0$ CV ($39.2 \pm 4.08\%$, $42.1 \pm 2.81\%$, $42.2 \pm 4.92\%$, and $38.9 \pm 3.25\%$) is the only distribution that the values are not significantly different among them.

Many studies are concerned with the f_oF_2 CV, and most of them were conducted in the equatorial region and Northern Hemisphere. For instance, Akala et al. (2010) presented the diurnal, seasonal, and solar activity impacts on the f_oF_2 CV over the Southeast Asian sector. The authors revealed that f_oF_2 is more susceptible to variability during the nighttime than the daytime and is characterized by a post-sunset peak (15–50%) and a post-midnight peak (18–68%). The authors found that the trend of the f_oF_2 variability does not follow any typical pattern on season. The f_oF_2 CV maximum occurs in June Solstice and September Equinox. Bilitza et al. (2004) studied f_oF_2 CV in two equatorial stations in the African sector for low, moderate, and high solar

Table 1
Seasonal Minimum, Maximum, and Average of the Coefficient of Variabilities (CV) Including the Corresponding Standard Deviation

CV (%)	Season	Minimum $\pm \sigma$ (%)	Maximum $\pm \sigma$ (%)	$\mu \pm \sigma$ (%)
f_oF_2 CV	December solstice	7.0 ± 0.24	23.0 ± 1.28	15.2 ± 4.7
	March equinox	9.4 ± 0.95	38.5 ± 1.36	20.0 ± 7.5
	June solstice	5.6 ± 2.26	19.0 ± 1.21	13.4 ± 2.8
	September equinox	19.6 ± 0.65	49.4 ± 1.90	31.3 ± 6.8
f_oE CV	December solstice	4.1 ± 0.32	6.6 ± 0.77	5.4 ± 0.8
	March equinox	5.7 ± 0.35	9.9 ± 1.49	6.9 ± 1.3
	June solstice	3.2 ± 0.25	8.2 ± 0.28	4.6 ± 1.4
	September equinox	4.8 ± 0.34	10.2 ± 1.79	6.5 ± 1.7
h_mF_2 CV	December solstice	4.3 ± 0.28	12.9 ± 1.19	7.7 ± 2.2
	March equinox	7.3 ± 0.91	14.4 ± 0.67	10.8 ± 1.8
	June solstice	5.3 ± 0.53	13.4 ± 1.76	9.5 ± 2.2
	September equinox	7.1 ± 1.12	17.4 ± 1.23	11.6 ± 2.8
$B0$ CV	December solstice	18.4 ± 1.82	39.2 ± 4.08	25.5 ± 5.8
	March equinox	20.9 ± 3.66	42.1 ± 2.81	31.7 ± 5.1
	June solstice	25.3 ± 4.61	42.2 ± 4.92	34.2 ± 4.8
	September equinox	23.4 ± 4.41	38.9 ± 3.25	30.9 ± 3.9

activities. Regarding their results during low solar activity only, which is the case here, the authors found that the CV is the lowest during daytime (5–15%) and increases during nighttime (15–30 %) for both stations. As the authors compared the data acquired at Korhogo (9.3° N, 5.4° W, dip angle = 0.67°) located in the equator and Ouagadougou (12° N, 1.8° W, dip angle = 15.9°) situated in the EIA crest, significant differences were observed in the f_oF_2 variability, being greater in the former station than in the second. Zhang et al. (2004) found that the variability in f_oF_2 is much lower during daytime hours than in nighttime hours, with the maximum variability occurring at presunrise hours at Hainan, China (19.4° N, 109.0° E, dip angle = 22.8°). We do not include the specific values here because Zhang et al. (2004) obtained the variability in terms of percentage interquartile values. The lower f_oF_2 CV values during daytime hours than nighttime hours are attributed by the authors to the steep electron density gradients caused by the onset and turn-off of solar ionization and superimposition of ionospheric F region irregularities (spread F) on the background electron density. At night, when the photochemical control is weaker and the ionospheric electron density is dependent on the recombination rate, the electron density is more sensitive to the meteorological activity as meridional winds. We have no reason to disagree with the preview conclusions, which is consistent, for example, with the mass plot shown in Figure 3a.

Inspection of Figure 4b shows that the diurnal variation of f_oE CV is characterized by a maximum at the sunrise. It decreases from the dawn values to a plateau of around 5 ± 1% between 12:00 UT and 22:00 UT in all seasons. Table 1 shows that f_oE CV spans from 3.2 ± 0.25% at 14:00 UT in June solstice to 10.2 ± 1.79% at 10:00 UT in September equinox. March equinox is the most variable season with an average of 6.9 ± 1.3%, and June solstice is the least variable season with an average of 4.6 ± 1.4%. These results reveal that the f_oE is the least variable parameter in our study, that is, the variability of the E region is less than that of the F region. The diurnal variation pattern of f_oE CV observed is due to the predominant control of photoionization and loss process that take place below the F_2 peak. It is expected a balance between the formation and recombination processes during daytime, which sets the E region into a quasi-stationary equilibrium leading to small f_oE CV. Both the daytime and nighttime seasonal patterns of the f_oE CV values agree closely with the results reported by Abe et al. (2013) at Ouagadougou during low solar activity. The authors found that the magnitude of the CV ranges from 3.0% observed at local noon to 7.8% observed during sunrise hours, higher magnitude in June solstice and the lowest magnitude in December solstice. Comparing their results with ours, we see that the variability over Santa Maria is slightly higher in magnitude than Ouagadougou. Since a permanent feature of the equatorial F region is the $\mathbf{E} \times \mathbf{B}$ dynamics caused by the equatorial electrojet and prereversal enhancement, we would expect larger day-to-day variability in Ouagadougou than in Santa Maria.

The diurnal variation pattern of h_mF_2 CV and $B0$ CV presented in Figures 4c and 4d, respectively, is more complicated when compared with f_oF_2 CV and f_oE CV. We note in general a presunrise, local midday, and a post-sunset peak for March equinox, June solstice, and September equinox. The presunrise and post-

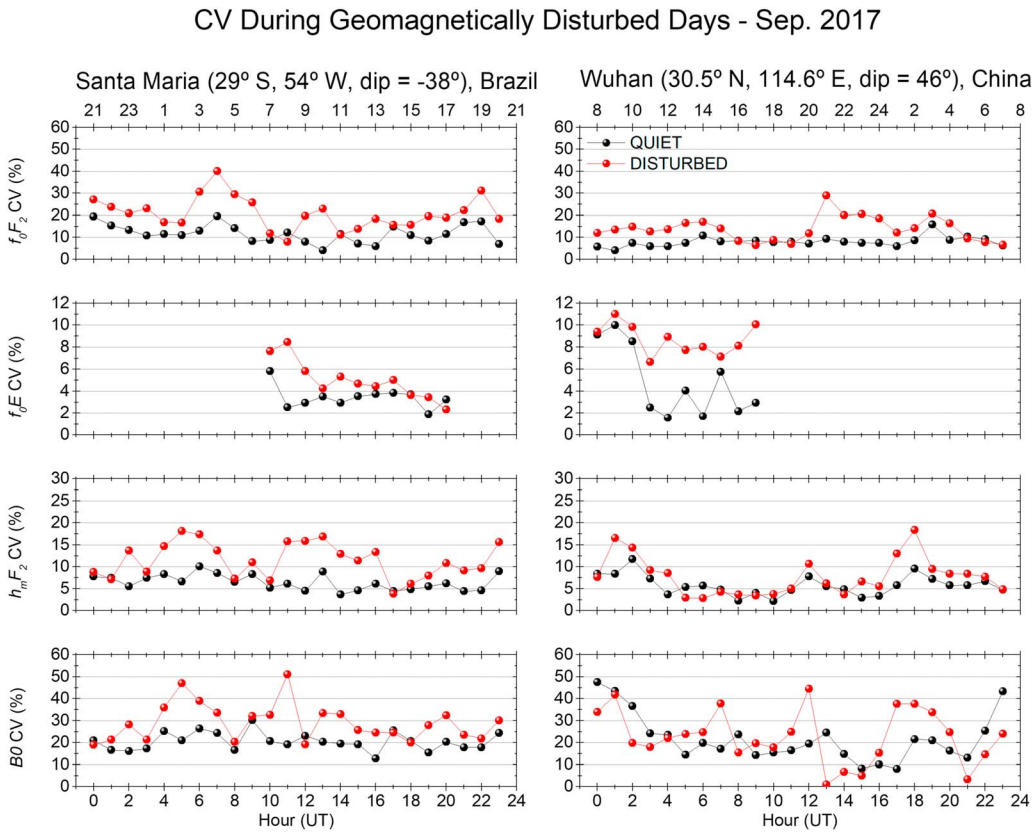

Figure 5. Coefficient of variability (CV) evaluated for the f_oF_2, f_oE, h_mF_2, and $B0$ parameters in the most disturbed days (red dots) and the quietest days (black dots) of September 2017 geomagnetic storm as a function of universal time for the Santa Maria (left panels) and Wuhan (right panels) stations. The local time scale for each station is at the top.

sunset peaks are not observed in December solstice for h_mF_2 CV. The occurrence time of the presunrise peak is shifted to later (9:00 UT) for $B0$ CV. From Table 1, we see that h_mF_2 CV ranges from 4.3 ± 0.28% at 5:00 UT in December solstice to 17.4 ± 1.23% at 14:00 UT in September equinox. The highest seasonal average of h_mF_2 CV equal to 11.6 ± 2.8% is detected in September equinox, while the least seasonal average of 7.7 ± 2.2% is detected in December solstice. Our findings reveal that the variability of h_mF_2 is much less than that observed in the f_oF_2 parameter. This is in line with the observations of Tsagouri et al. (2018) over seven ionospheric locations in the Northern Hemisphere in the Year 2002. The authors found that on average, the CV is about 14% and 7% for f_oF_2 and h_mF_2, respectively. There is no expressive difference between the variabilities detected here in h_mF_2 and those reported by Altadill (2007) using ionosonde data acquired from January 1995 to December 2005 at the Ebro Observatory (40.8° N, 0.5° E). The author found that h_mF_2 CV ranges from 10% to 20%, larger by night than by day with an average of 13.3%.

Concerning $B0$ CV shown in Table 1, the minimum observed value is 18.4 ± 1.82% at 3:00 UT in December solstice. We are not able to determine the season with the maximum variability since the 39.2 ± 4.08%, 42.1 ± 2.81%, 42.2 ± 4.92%, and 38.9 ± 3.25% values are not significantly different at the 0.05 level from the Kruskal-Wallis test, as mentioned before. The highest seasonal average of $B0$ CV is 34.2 ± 4.8% detected in June solstice, and the least is 25.5 ± 5.8% observed in December solstice. Therefore, we find that the most variable parameter in our work is $B0$. For the $B0$ CV obtained in Hainan, China, Zhang et al. (2004) found that it has a minimum value at hours after sunrise and sunset in winter and equinox seasons, while it has maximum values around port-midnight hours.

3.3. Ionospheric Variabilities During Geomagnetically Disturbed Days

In order to further investigate the geomagnetic activity impacts on the ionospheric variabilities in the central region of the SAMA, we evaluated the CV during geomagnetically disturbed days and compare it with the

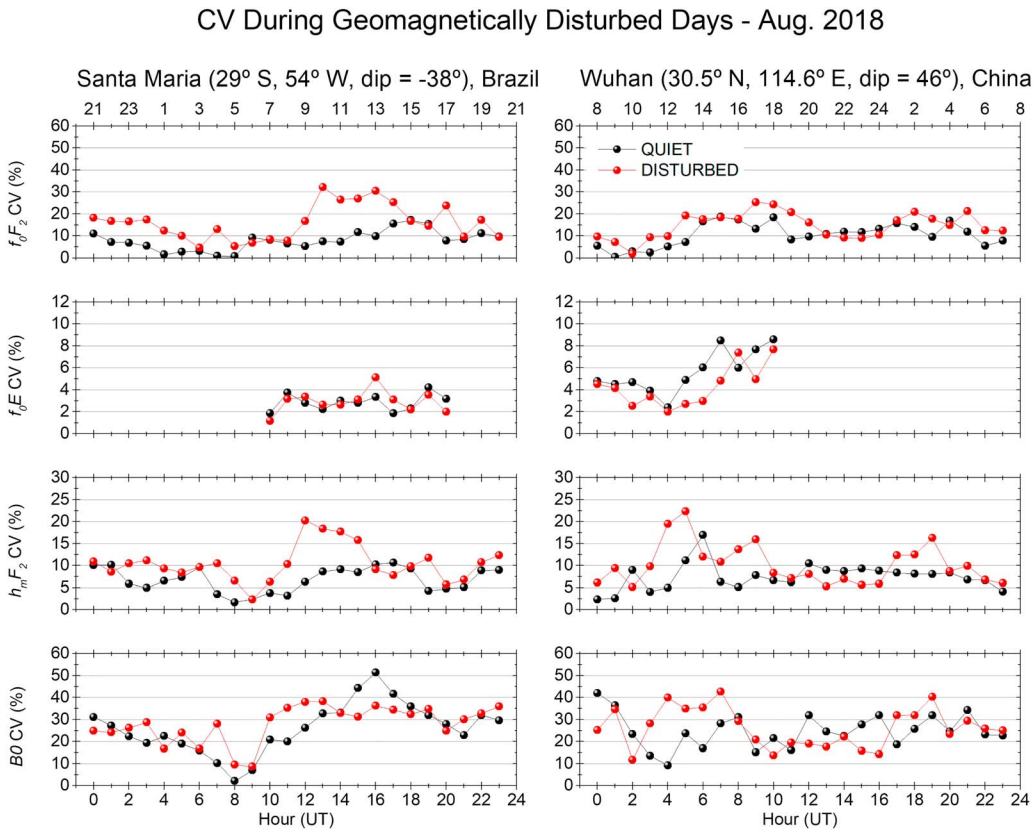

Figure 6. Same as Figure 5 but for August 2018 geomagnetic storm.

geomagnetically quiet days of the same month in two case studies. The first case study refers to the geomagnetic storm of 7 September 2017, which Disturbance storm-time (Dst) index achieved −142 nT at 2 UT on 8 September and −122 nT at 15 UT of the same day. The disturbed CV calculated from data acquired during the geomagnetically disturbed days (7, 8, 15, 27, and 28) of September 2017 is compared with the CV obtained from the geomagnetically quiet days (9, 22, 23, 25, and 26) of the month. The variabilities evaluated for Santa Maria are compared with the CV obtained from ionospheric data acquired at the Wuhan Ionospheric Observatory for the same days. The estimated hourly CV is presented in the left panels of Figure 5 for Santa Maria and in the right panels for Wuhan. The resulted diurnal variation of CV considering the active days is shown by the red dots, while the CV averaged from parameters measured in quiet days is shown by black dots.

The enhancement of the variability in all parameters considering geomagnetically disturbed days is significant over Santa Maria when compared with the CV evaluated with geomagnetically quiet days. In average, f_oF_2 CV is 20.9 ± 7.3% during disturbed conditions and 11.7 ± 4.1% during geomagnetic quiet days. Regarding the f_oE CV, the variability increased to 5.0 ± 1.8% from 3.4 ± 1.0%. The h_mF_2 CV is on average 11.5 ± 4% in disturbed conditions while only 6.5 ± 1.8% in quiet condition. With respect to the most variable parameter in our study, *B*0 CV achieved 29.0 ± 8.5% during geomagnetically disturbed days, which is higher than the 20.4 ± 4.1% obtained from geomagnetically quiet days. These results clearly indicate that during geomagnetically disturbed periods, the ionosphere over Santa Maria is subject of this important source of variability in addition to the meteorological source present in the geomagnetically quiet period.

Regarding the CV estimated over the Wuhan station, in general, CV also shows an enhancement in the disturbed days when compared with quiet days. In average, the f_oF_2 CV is 13.8 ± 5.4% during disturbed conditions and 8.0 ± 2.3% during geomagnetic quiet days. The f_oE CV increased to 8.7 ± 1.4% from 4.8 ± 3.3%. The h_mF_2 CV is on average 7.7 ± 4.3% in disturbed conditions while 5.8 ± 2.3% in the quiet condition. We do not observe a large enhancement of *B*0 CV over Wuhan during the geomagnetically disturbed days. It increased to only 22.8 ± 12.2% as compared with 21.7 ± 10.9% during geomagnetically quiet days.

Table 2
Average of the Coefficient of Variabilities (CV) Including the Corresponding Standard Deviation for the Selected Ionospheric Parameters Over Santa Maria and Wuhan During the Geomagnetically Quiet and Disturbed Days of 7 September 2017 and 26 August 2018 Geomagnetic Storms

Geomagnetic storm	CV (%)	Santa Maria, Brazil		Wuhan, China	
		Disturbed days	Quiet days	Disturbed days	Quiet days
7 September 2017	f_oF_2 CV	20.9 ± 7.3	11.7 ± 4.1	13.8 ± 5.4	8.0 ± 2.3
	f_oE CV	5.0 ± 1.8	3.4 ± 1.0	8.7 ± 1.4	4.8 ± 3.3
	h_mF_2 CV	11.5 ± 4.0	6.5 ± 1.8	7.7 ± 4.3	5.8 ± 2.3
	$B0$ CV	29.0 ± 8.5	20.4 ± 4.1	22.8 ± 12.2	21.7 ± 10.9
26 August 2018	f_oF_2 CV	16.1 ± 7.9	7.9 ± 4.4	14.7 ± 5.9	10.6 ± 5.3
	f_oE CV	2.9 ± 1.0	2.8 ± 0.6	4.3 ± 1.9	5.6 ± 2.0
	h_mF_2 CV	10.4 ± 4.2	6.8 ± 2.8	10.2 ± 4.6	7.5 ± 3.1
	$B0$ CV	28.1 ± 8.3	26.1 ± 11.4	26.3 ± 8.9	24.8 ± 7.8

In order to confirm the same trend observed for the September 2017 geomagnetic storm, we also present another case study in Figure 6. The Dst index recorded in 26 August 2018 geomagnetic storm indicates a sharp drop to a minimum of −174 nT between 7 and 8 UT on 26 August. Following the same strategy of the first case study, we calculated the CV during the geomagnetically disturbed days (15, 17, 20, 26, and 27) of August 2018 and compare it with the CV obtained from the geomagnetically quiet days (6, 10, 13, 14, and 23) of the same month. The results of both cases studies are placed in Table 2. Repeatedly, we note that in general, the degree of variabilities also increases in all parameters in both stations, that is, Santa Maria and Wuhan. The only exception is for f_oE CV at Wuhan, which presents higher value during the quiet period as compared with the disturbed period. However, this difference is not significant since it lies within the standard deviation of the mean values.

Another interesting point that comes from the analysis of Figures 5 and 6 and Table 2 is that the variabilities during the geomagnetic storms are higher over Santa Maria than Wuhan. It can be explained due to the presence of the SAMA in the former station. The increase in the ionization production (rising the f_oF_2) over Santa Maria is explained by the trapped and azimuthally drifting of energetic particles coming deeper down into the dense neutral atmosphere through the low magnetic field intensity (conserving the second adiabatic invariant) while bouncing between hemispheres. Even though the September 2017 geomagnetic storm was less intense than the August 2018 as indicated by the Dst index, the higher variability detected in the ionospheric parameters during the former storm can be explain by the fact that it consisted of two consecutive magnetic storms separated in time by ~13 hr, as well explained by Blagoveshchensky et al. (2019).

Some of the aforementioned works studied the influence of geomagnetic activity on the ionospheric variability. For example, Forbes et al. (2000) found that the f_oF_2 CV increases with the geomagnetic activity, considering data of two solar cycles. However, Araujo-Pradere et al. (2005) argued that the variability tended to increase with geomagnetic activity at low and middle latitudes in June solstice and equinoxes but remained fairly constant in December solstice.

The geometry of the geomagnetic field in the SAMA region associated with the plasma transport along the field and perpendicular to it by winds makes the interpretation of the large amount of variability in the observed ionospheric parameters difficult. The meridional winds may transport the plasma in altitude and latitude, given the geometry of the geomagnetic field. The results of the CV provided in Figure 3 is attributed to the neutral atmosphere as the main source of ionospheric variability. The detailed explanation of the "meteorological" as a main source of the variability remains a challenge due to the lack of measurements in the south of Brazil, but the average values of the ionospheric parameters shown in this work are what models driven by climatological parameters should attempt to reproduce.

4. Conclusions

We have presented the first study of the diurnal, seasonal, and ionospheric variability in the f_oF_2, h_mF_2, $B0$, and f_oE parameters over Santa Maria (29.7° S, 53.7° W, dip angle = −37°), a station located near the central region of the SAMA. The ionospheric parameters were recorded with a time resolution of 5 min from 1

September 2017 to 30 August 2018, totalizing 309 days by a DPS-4D. The diurnal variation patterns show that f_oF_2, f_oE, and $B0$ values are higher during daytime hours as compared to nighttime hours. In general, h_mF_2 values present opposite behavior, that is, the nighttime values are higher than those of the daytime values except for short periods around 9:00 UT in June solstice and around 14:30 UT in December solstice. It also observed a remarkable mean difference in all parameters between December and June solstices, revealing a possible presence of the annual asymmetry, and a lesser extent difference between March and September equinoxes. Comparing our results with the finds from other stations located in the EIA crests and outside the SAMA's control, we found that the effects of the EIA are more intense in the ionospheric parameters than the ones caused by the SAMA.

The CV is used as an index to quantitatively describe the ionospheric variability of each parameter. The whole year analyzed is characterized by low solar and geomagnetic activity, which is an important advantage to estimate the relative contribution of different sources under enough rigid restrictions on the threshold level of the geomagnetic activity. Considering the low $F_{10.7}$ and sunspot number during the period analyzed and excluding the geomagnetically disturbed data, the f_oF_2 CV, f_oE CV, h_mF_2 CV, and $B0$ CV obtained should be mainly due to the meteorological sources. The diurnal analysis reveals that the ionosphere in the central region of the SAMA is more susceptible to variability during nighttime than daytime hours. The f_oF_2 CV ranges from $5.6 \pm 2.26\%$ detected in June solstice to $49.4 \pm 1.90\%$ observed in September equinox. In average, f_oF_2 is more variable during September equinox ($31.3 \pm 6.8\%$) and less variable in June solstice ($13.4 \pm 2.8\%$). The f_oE CV is characterized by a maximum at the sunrise, spanning from $3.2 \pm 0.25\%$ in June solstice to $10.2 \pm 1.79\%$ in September equinox. The highest variabilities of f_oE occur in March equinox ($6.9 \pm 1.3\%$) and the lowest in June solstice ($4.\ 6 \pm 1.4\%$). These results reveal that the f_oE is the least variable parameter in our study, that is, the variability of the E region is less than that of the F region. Regarding the h_mF_2 CV, it ranges from $4.3 \pm 0.28\%$ in December solstice to $17.4 \pm 1.23\%$ in September equinox. The highest seasonal average of h_mF_2 is detected in September equinox ($11.6 \pm 2.8\%$), while the least seasonal average is detected in December solstice ($7.7 \pm 2.2\%$). Our findings reveal that the variability of h_mF_2 is much less than that observed in the f_oF_2 parameter. Finally, the minimum $B0$ CV is 18.4 ± 1.82 % observed in December solstice. We are not able to determine the season with the highest $B0$ variability since the maximum $B0$ CV values are not significantly different among them. In average, the highest variability is detected in June solstice ($34.2 \pm 4.8\%$) and the least one in December solstice ($25.5 \pm 5.8\%$). Therefore, $B0$ is the most analyzed variable parameter in our work.

The geomagnetic activity impacts on the ionospheric variabilities in Santa Maria, Brazil, are evaluated during two geomagnetic storms, and the results are compared with Wuhan, China. The estimated CV is enhanced during geomagnetically disturbed days in both stations and reveals that the variability in the former stations is generally higher on average. This fact may be explained by the presence of the SAMA in the Brazilian low-latitude station, which leads to an increase of the ionization production in the ionosphere. It, in turn, is caused by the trapped and azimuthally drifts of energetic particles that precipitate into the dense neutral atmosphere through the low magnetic field intensity (conserving the second adiabatic invariant) while bouncing between hemispheres. Therefore, our results clearly indicate that the ionosphere over Santa Maria is subject of this important source of variability during geomagnetically disturbed periods in addition to the meteorological source present in the geomagnetically quiet periods.

Acknowledgments
J. Moro would like to acknowledge the China-Brazil Joint Laboratory for Space Weather (CBJLSW), National Space Science Center (NSSC), and Chinese Academy of Sciences (CAS) for supporting his Postdoctoral fellowship and the National Council for Scientific and Technological Development (CNPq) for the Grant 429517/2018-01. C. M. Denardini thanks CNPq for the fellowship under the 03121/2014-9. L. C. A. Resende would like to acknowledge the financial support from CNPq process 169404/2017-0 and the CBJLSW for supporting her Postdoctoral fellowship. R. P. Silva acknowledges the support from CNPq for the Grant 300329/2019-9. N. J. Schuch thanks CNPq for the fellowship under the 300886/2016-0. The authors thank the referees for their assistance in evaluating this paper. The authors also thank the OMNIWEB (https://omniweb.gsfc.nasa.gov/form/dx1.html) for providing $F_{10.7}$ index, sunspot number, and the *Kp* index used in the classification of the days. The Digisonde data from Santa Maria can be downloaded upon registration at the Embrace webpage from INPE Space Weather Program (http://www2.inpe.br/climaespacial/portal/en/). The Digisonde data from Wuhan can be downloaded upon registration at the Data Centre for Meridian Space Weather Monitoring Project (https://data.meridianproject.ac.cn/). We acknowledge the use of data from the Chinese Meridian Project. J. Moro and N. J. Schuch acknowledge the support of the Federal University of Santa Maria (UFSM) Central Administration. J. Moro acknowledges David Kitrosser and Ryan Hamel from Lowell Digisonde International for their assistance with the Digisonde.

References

Abdu, M. A. (2001). Outstanding problems in the equatorial ionosphere–thermosphere electrodynamics relevant to spread F. *Journal of Atmospheric and Terrestrial Physics*, *63*(9), 869–884. https://doi.org/10.1016/S1364-6826(00)00201-7

Abdu, M. A., Batista, I. S., Carrasco, A. J., & Brum, C. G. M. (2005). South Atlantic Magnetic Anomaly ionization: A review and a new focus on electrodynamics effects in the equatorial ionosphere. *Journal of Atmospheric and Solar-Terrestrial Physics*, *67*(17-18), 1643–1657. https://doi.org/10.1016/j.jastp.2005.01.014

Abdu, M. A., Batista, I. S., Reinisch, B. W., de Souza, J. R., Sobral, J. H. A., Pedersen, T. R., et al. (2009). Conjugate Point Equatorial Experiment (COPEX) campaign in Brazil: Electrodynamics highlights on spread *F* development conditions and day-to-day variability. *Journal of Geophysical Research*, *114*, A04308. https://doi.org/10.1029/2008JA013749

Abe, O. E., Rabiu, A. B., & Adeniyi, J. O. (2013). Variability of f_oE in the equatorial ionosphere with solar activity. *Advances in Space Research*, *51*, 69–75.

Akala, A. O., Adeloye, A. B., & Somoye, E. O. (2010). Ionospheric foF2 variability over the Southeast Asian sector. *Journal of Geophysical Research*, *115*, A09329. https://doi.org/10.1029/2010JA015250

Altadill, D. (2007). Time/altitude electron density variability above Ebro, Spain. *Advances in Space Research*, *39*(5), 962–969. https://doi.org/10.1016/j.asr.2006.05.031

Ameen, M. A., Khursheed, H., Jabbar, M. A., Ali, M. S., & Chishtie, F. (2018). Variation of hmF2 and NmF2 deduced from DPS-4 over Multan (Pakistan) and their comparisons with IRI-2012 & IRI-2016 during the deep solar minimum between cycles 23 & 24. *Advances in Space Research*, *61*(7), 1726–1735. https://doi.org/10.1016/j.asr.2018.01.043

Araujo-Pradere, E. A., Fuller-Rowell, T. J., Codrescu, M. V., & Bilitza, D. (2005). Characteristics of the ionospheric variability as a function of season, latitude, local time, and geomagnetic activity. *Radio Science*, *40*, RS5009. https://doi.org/10.1029/2004RS003179

Balan, N., Otsuka, Y., & Fukao, S. (1997). New aspects in the annual variation of the ionosphere observed by the MU radar. *Journal of Geophysical Research*, *24*(18), 2287–2290. https://doi.org/10.1029/97GL02184

Batista, I. S., & Abdu, M. A. (2004). Ionospheric variability at Brazilian low and equatorial latitudes: Comparison between observations and IRI model. *Advances in Space Research*, *34*(9), 1894–1900. https://doi.org/10.1016/j.asr.2004.04.012

Batista, I. S., Sastri, J. H., de Medeiros, R. T., & Abdu, M. A. (1997). Nighttime thermospheric meridional winds at Cachoeira Paulista (23°S, 45°W): Evidence for effects of the equatorial midnight pressure bulge. *Journal of Geophysical Research*, *102*(A9), 20,059–20,062. https://doi.org/10.1029/97JA01387

Bello, S. A., Abdullah, M., Hamid, N. S. A., Reinisch, B. W., Yoshikawa, A., & Fujimoto, A. (2019). Response of ionospheric profile parameters to equatorial electrojet over Peruvian station. *Earth and Space Science*, *6*(4), 617–628. https://doi.org/10.1029/2018EA000537

Bilitza, D., Obrou, O. K., Adeniyi, J. O., & Oladipo, O. (2004). Variability of f_oF2 in the equatorial ionosphere. *Advances in Space Research*, *34*(9), 1901–1906. https://doi.org/10.1016/j.asr.2004.08.004

Bilitza, D., Radicella, S. M., Reinisch, B. W., Adeniyi, J. O., Mosert Gonzalez, M. E., Zhang, S. R., & Obrou, O. (2000). New *B*0 and *B*1 models for IRI. *Advances in Space Research*, *25*(1), 89–95. https://doi.org/10.1016/S0273-1177(99)00902-3

Blagoveshchensky, B. V., Sergeeva, M. A., & Corona-Romero, P. (2019). Features of the magnetic disturbance on September 7–8, 2017 by geophysical data. *Advances in Space Research*, *64*(1), 171–182. https://doi.org/10.1016/j.asr.2019.03.037

Denardini, C. M., Chen, S. S., Resende, L. C. A., Moro, J., Bilibio, A. V., Fagundes, P. R., et al. (2018). The embrace magnetometer network for South America: First scientific results. *Radio Science*, *53*, 379–393. https://doi.org/10.1002/2018RS006540

Forbes, J. M., Palo, S. E., & Zhang, X. (2000). Variability of the ionosphere. *Journal of Atmospheric and Solar-Terrestrial Physics*, *62*(8), 685–693. https://doi.org/10.1016/S1364-6826(00)00029-8

Gong, Y., Zhou, Q., Zhang, S., Aponte, N., Sulzer, M., & Gonzalez, S. (2012). Midnight ionosphere collapse at Arecibo and its relationship to the neutral wind, electric field, and ambipolar diffusion. *Journal of Geophysical Research*, *117*, A08332. https://doi.org/10.1029/2012JA017530

Hargreaves, J. K. (1995). *The solar-terrestrial environment: An introduction to geospace—The science of the terrestrial upper atmosphere, ionosphere, and magnetosphere. Cambridge Atmospheric and Space Science Series*.

Huang, X., & Reinisch, B. W. (2001). Vertical electron content from ionograms in real time. *Radio Science*, *36*(2), 335–342.

Kalita, B. R., Bhuyan, P. K., & Yoshikawa, A. (2015). NmF2 and hmF2 measurements at 95° E and 127° E around the EIA northern crest during 2010–2014. *Earth, Planets and Space*, *67*(1), 186. https://doi.org/10.1186/s40623-015-0355-3

Kruskal, W. H., & Wallis, W. A. (1952). Use of ranks in one-criterion variance analysis. *Journal of the American Statistical Association*, *47*(260), 583–621. https://doi.org/10.1080/01621459.1952.10483441

Lee, C. C., & Reinisch, B. W. (2012). Variations in equatorial F2-layer parameters and comparison with IRI-2007 during a deep solar minimum. *Journal of Atmospheric and Solar-Terrestrial Physics*, *74*, 217–223. https://doi.org/10.1016/j.jastp.2011.11.002

Liu, L., Wan, W., Ning, B., & Zhang, M.-L. (2009). Climatology of the mean total electron content derived from GPS global ionospheric maps. *Journal of Geophysical Research*, *114*, A06308. https://doi.org/10.1029/2009JA014244

McNamara, L. F., Retterer, J. M., Abdu, M. A., Batista, I. S., & Reinisch, B. W. (2008). F2 peak parameters, drifts and spread F derived from digisonde ionograms for the COPEX campaign in Brazil. *Journal of Atmospheric and Solar-Terrestrial Physics*, *70*(8-9), 1144–1158. https://doi.org/10.1016/j.jastp.2008.02.001

Medvedeva, I., & Ratovsky, K. (2015). Studying atmospheric and ionospheric variabilities from long-term spectrometric and radio sounding measurements. *Journal of Geophysical Research: Space Physics*, *120*, 5151–5159. https://doi.org/10.1002/2015JA021289

Moro, J., Denardini, C. M., Abdu, M. A., Correia, E., Schuch, N. J., & Makita, K. (2012). Latitudinal dependence of cosmic noise absorption in the ionosphere over the SAMA region during the September 2008 magnetic storm. *Journal of Geophysical Research*, *117*, A06311. https://doi.org/10.1029/2011JA017405

Moro, J., Denardini, C. M., Abdu, M. A., Correia, E., Schuch, N. J., & Makita, K. (2013). Correlation between the cosmic noise absorption calculated from the SARINET data and energetic particles measured by MEPED: Simultaneous observations over SAMA region. *Advances in Space Research*, *51*, 11,692–11,700.

Moro, J., Denardini, C. M., Resende, L. C. A., Chen, S. S., & Schuch, N. J. (2016a). Equatorial *E* region electric fields at the dip equator: 1. Variabilities in eastern Brazil and Peru. *Journal of Geophysical Research: Space Physics*, *121*, 10,220–10,230. https://doi.org/10.1002/2016JA022751

Moro, J., Denardini, C. M., Resende, L. C. A., Chen, S. S., & Schuch, N. J. (2016b). Equatorial *E* region electric fields at the dip equator: 2. Seasonal variabilities and effects over Brazil due to the secular variation of the magnetic equator. *Journal of Geophysical Research: Space Physics*, *121*, 10,231–10,240. https://doi.org/10.1002/2016JA022753

Moro, J., Resende, L. C. A., Denardini, C. M., Xu, J., Batista, I. S., Andrioli, V. F., et al. (2017). Equatorial *E* region electric fields and sporadic *E* layer responses to the recovery phase of the November 2004 geomagnetic storm. *Journal of Geophysical Research: Space Physics*, *122*, 12,517–12,533. https://doi.org/10.1002/2017JA024734

Ouattara, F., Amory-Mazaudier, C., Fleury, R., Lassudrie Duchesne, P., Vila, P., & Petitdidier, M. (2009). West African equatorial ionospheric parameters climatology based on Ouagadougou ionosonde station data from June 1966 to February 1998. *Annales Geophysicae*, *27*(6), 2503–2514. https://doi.org/10.5194/angeo-27-2503-2009

Reinisch, B. W., Galkin, I. A., Khmyrov, G. M., Kozlov, A. V., Bibl, K., Lisysyan, I. A., et al. (2009). The new Digisonde for research and monitoring applications. *Radio Science*, *44*, RS0A24. https://doi.org/10.1029/2008RS004115

Resende, L. C. A., Batista, I. S., Denardini, C. M., Carrasco, A. J., de Fátima Andrioli, V., Moro, J., et al. (2016). Competition between winds and electric fields in the formation of blanketing sporadic E layers at equatorial regions. *Earth, Planets and Space*, *68*(1). https://doi.org/10.1186/s40623-016-0577-z

Rishbeth, H., & Mendillo, M. (2001). Patterns of F2-layer variability. *Journal of Atmospheric and Solar-Terrestrial Physics*, *63*(15), 1661–1680. https://doi.org/10.1016/S1364-6826(01)00036-0

Rishbeth, H., & Müller-Wodarg, I. C. F. (2006). Why is there more ionosphere in January than in July? The annual asymmetry in the F2-layer. *Annals of Geophysics*, *24*(12), 3293–3311. https://doi.org/10.5194/angeo-24-3293-2006

Romero-Hernandez, E., Denardini, C. M., Takahashi, H., Gonzalez-Esparza, J. A., Nogueira, P. A. B., de Padua, M. B., et al. (2018). Daytime ionospheric TEC weather study over Latin America. *Journal of Geophysical Research: Space Physics*, *123*, 10,345–10,357. https://doi.org/10.1029/2018JA025943

Shim, J. S., Scherliess, L., Schunk, R. W., & Thompson, D. C. (2010). Neutral wind and plasma drift effects on low and middle latitude total electron content. *Journal of Geophysical Research*, *115*, A04307. https://doi.org/10.1029/2009JA014488

Somoye, E. O., & Akala, A. O. (2011). Comparison of diurnal seasonal and latitudinal effect of MUF VR and NmF2 VR during some solar cycle epochs. *Advances in Space Research*, *47*(12), 2182–2187. https://doi.org/10.1016/j.asr.2010.11.005

Titheridge, J. E. (2000). Modelling the peak of the ionospheric E-layer. *Journal of Atmospheric and Solar-Terrestrial Physics*, *62*(2), 93–114. https://doi.org/10.1016/S1364-6826(99)00102-9

Tsagouri, I., Goncharenko, L., Shim, J. S., Belehaki, A., Buresova, D., & Kuznetsova, M. M. (2018). Assessment of current capabilities in modeling the ionospheric climatology for space weather applications: foF2 and hmF2. *Space Weather*, *16*, 1930–1945. https://doi.org/10.1029/2018SW002035

Wang, C. (2010). New chains of space weather monitoring stations in China. *Space Weather*, *8*, S08001. https://doi.org/10.1029/2010SW000603

Zhang, M. L., Shi, J. K., Wang, X., & Radicella, S. M. (2004). Ionospheric variability at low latitude station: Hainan, China. *Advances in Space Research*, *34*(9), 1860–1868. https://doi.org/10.1016/j.asr.2004.04.005

Zhang, S.-R., & Holt, J. M. (2008). Ionospheric variability from an incoherent scatter radar long-duration experiment at Millstone Hill. *Journal of Geophysical Research*, *113*, A03310. https://doi.org/10.1029/2007JA012639

Zou, L., Rishbeth, H., Muller-Wodarg, I. C. F., Aylward, A. D., Millward, G. H., Fuller-Rowell, T. J., et al. (2000). Annual and semiannual variations in the ionospheric F2-layer: I. Modelling. *Annals of Geophysics*, *18*(8), 927–944. https://doi.org/10.1007/s00585-000-0927-8